Journal of Alloys and Compounds 509 (2011) 2697–2702

Contents lists available at ScienceDirect

Journal of Alloys and Compounds

journal homepage: www.elsevier.com/locate/jallcom

Phase transformations in the B2 phase of Co-rich Co–Al binary alloys

K. Niitsu, T. Omori, M. Nagasako, K. Oikawa, R. Kainuma*, K. Ishida

Department of Materials Science, Graduate School of Engineering, Tohoku University, 6-6-02 Aoba-yama, Sendai 980-8579, Japan

ARTICLE INFO

Article history:
Received 17 May 2010
Received in revised form
17 November 2010
Accepted 22 November 2010
Available online 30 November 2010

Keywords:
Metals
Scanning and transmission electron microscopy
Magnetic measurements

ABSTRACT

Phase transformations in the β (B2) phase of Co–21 and –23 at.% Al alloys were examined using transmission electron microscopy, energy dispersive X-ray spectroscopy and differential scanning calorimetry. The microstructures obtained from as-quenched specimens were found to be strongly affected by the quenching condition. While relatively thick sheet-specimens with a lower quenching rate showed bainitic plate precipitates with a fcc structure, a martensite-like structure was observed by optical microscopy in relatively thin specimens with a higher quenching rate. Regardless of the quenching condition, a spinodal-like microstructure composed of A2 and B2 phases was also detected and the A2 phase changed to a metastable hcp phase during further aging.

1. Introduction

Co–Al is one of the most important binary systems for many Co-based functional alloys, such as hard magnets [1], shape memory material [2,3] and heat-resistant materials [4]. There are three solid phases, namely α-Co (A1: fcc solid solution), ε-Co (A3: hcp solid solution) and β-CoAl (B2: ordered bcc) phases, in the Co-rich portion of the Co–Al binary system, as shown in Fig. 1 [5]. In both the α and β, phases the high solubility at high temperatures remarkably decreases with decreasing temperature at around 800 °C and 1100 °C, respectively. To date, some metastable phases precipitating in these solid-solution phases have been reported. In the α solid-solution aged at 600 °C, a Co_3Al ($L1_2$: ordered fcc) metastable phase appears with a cuboidal microstructure similar to that in the Ni_3Al phase observed in the Ni-based superalloys [6]. On the other hand, very fine ε plates have been confirmed to precipitate into the supercooled β phase at elevated temperatures even in the α + β two-phase region of the phase diagram and to cause a high coercivity [7,8]. This ε + β alloy with high coercivity is known as Malcolloy [1,7,8]. Furthermore, thermodynamic analysis has suggested that metastable phase separation of A2 and B2 phases occurs in the same α + β two-phase region of the phase diagram [9], and actually the metastable A2 phase in β phase alloys has experimentally been confirmed by Kozakai et al. [10] as plotted with open circles in Fig. 1. Recently, the present author's group has experimentally determined the Co–Fe–Al ternary phase diagrams at some elevated temperatures [11] and estimated metastable equilibrium compositions in the A2 + B2 two-phase region of Co–Al binary system by extrapolation from the ternary equilibrium data, as shown by the closed circles in Fig. 1. This suggests that the large α + β two-phase concentration region not including a stable $L1_2$ phase in the Co–Al phase diagram, which is different from the Ni–Al phase diagram, is due to the existence of the A2 + B2 metastable phase equilibrium. In the Co–Al system, there is another important point different from that in the Ni–Al system, which is martensitic transformation induced by quenching from the β phase region [12,13]. Although the Ni-rich β-NiAl alloys are known to show a martensitic transformation from B2 to $L1_0$ (ordered fct) phase [14], no martensitic transformation from the B2 phase has been reported in binary β-CoAl alloys. In the present work, the phase transformations in Co-rich β alloys induced by quenching from the β phase and by further aging were experimentally investigated.

2. Experimental procedures

Co–21 and –23 at.% Al alloys were prepared from Co (99.9 wt.%) and Al (99.7 wt.%) by induction melting under an Ar atmosphere. Co–21 and –23 at.% Al ingots were cut into sheets about 5 mm thick (sample A and sample B, respectively) and a specimen of Co–23 at.% Al with a thickness of 1 mm was also prepared (sample C). These samples were sealed in quartz tubes evacuated and backfilled with Ar gas. Solution heat treatment was carried out at 1380 °C for 1 h, followed by quenching in ice water. For some specimens, aging heat treatments were subsequently carried out by heating from room temperature (RT) at heating rates of 5 and 10 °C/min. Microstructural observations were carried out by optical microscope using an etchant composed of the same ratio of HCl and HNO_3, transmission electron microscopy (TEM; JEOL JEM-2000EXII) at 200 kV and high-resolution electron microscopy (HREM; JEOL JEM-3010) at 300 kV. Thin foils for TEM and HREM were prepared by jet-polishing in a solution of 72% acetic acid, 12% ethanol, 8% ethylene glycol and 8% perchloric acid. Composition analysis was also conducted by TEM-EDS (energy dispersive X-ray spectroscopy), and the crystal structures of the constituent

* Corresponding author at: Department of Materials Science, Graduate School of Engineering, Tohoku University, 6-6-02 Aoba Yama, Sendai, Miyagi 980-8579, Japan. Tel.: +81 22 795 7321; fax: +81 22 795 7323.

0925-8388/$ – see front matter © 2010 Elsevier B.V. All rights reserved.
doi:10.1016/j.jallcom.2010.11.130

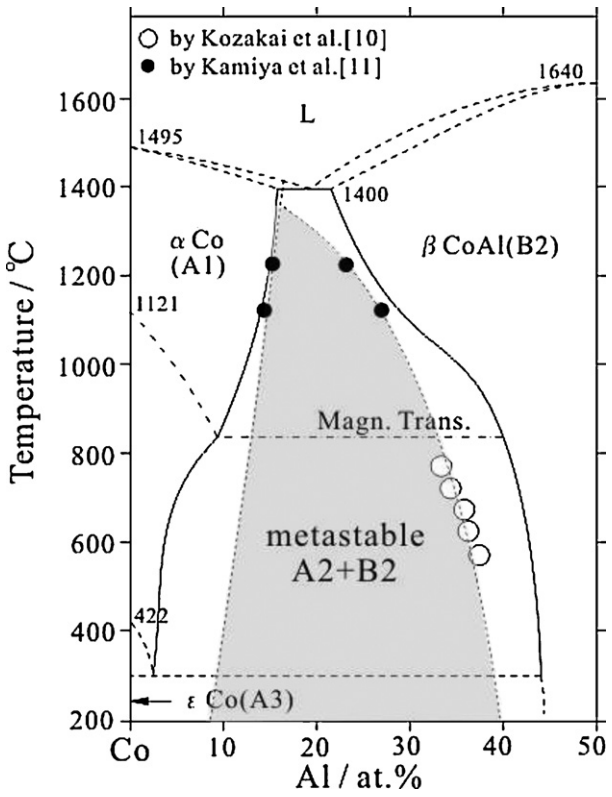

Fig. 1. Co-rich portion of Co–Al binary phase diagram including a metastable A2 + B2 two-phase region.

phases were identified by X-ray diffraction (XRD). The transformation temperatures were determined by differential scanning calorimetric (DSC) at heating rates of 1, 5 and 10 °C/min. The magnetic properties were measured by a vibrating sample magnetometer (VSM) at a heating rate of 5 °C/min.

3. Results and discussion

3.1. Martensitic and bainitic transformations

Fig. 2 shows optical micrographs of (a) sample B (5 mm in thickness), (b) sample C (1 mm in thickness) and (c) the bright field image (BFI) from the $[1\,1\,0]_{bcc}$ direction of the parent phase of sample C. Here, these samples were quenched from 1380 °C. The microstructures are different between the samples with different thicknesses, which is considered to result from the difference in the quenching rate because it should be higher in the thin specimen than in the thick one. As shown in Fig. 2(a) and (b), sample B shows thin plates, while a martensite-like structure can be partially observed in sample C. Note that sample A (5 mm in thickness) showed almost the same microstructure as sample B shown in Fig. 2(a). A very fine two-phase structure resembling spinodal decomposition, as shown in Fig. 2(c), was observed in the parent phases of all samples quenched from 1380 °C, which means that this phase separation cannot be suppressed by water quenching.

Fig. 3(a) and (b) shows the BFI from the $[1\,1\,0]_{bcc}$ direction of sample A quenched from 1380 °C and the concentration profile along a horizontal line in Fig. 3(a) obtained by using TEM-EDX. The composition of the thin plate is about Co–13 at.% Al, which is clearly lower than that of the matrix, and a concentration spike of Al is formed in the β matrix zone neighboring the plate. On the other hand, a higher magnification BFI for another plate and its corresponding SADP are shown in Fig. 3(c) and (d), respectively. High density of plane defects is observed in Fig. 3(c), and the SADP of Fig. 3(e) enlarging the square region in Fig. 3(d) shows a twin relation, which suggests that these plane defects are micro-twins. It is also confirmed from Fig. 3(d) that the plate has a fcc structure. Judging from these microstructure and composition analyses, this plate would be a product of bainitic transformation including both displacive and diffusional characteristics.

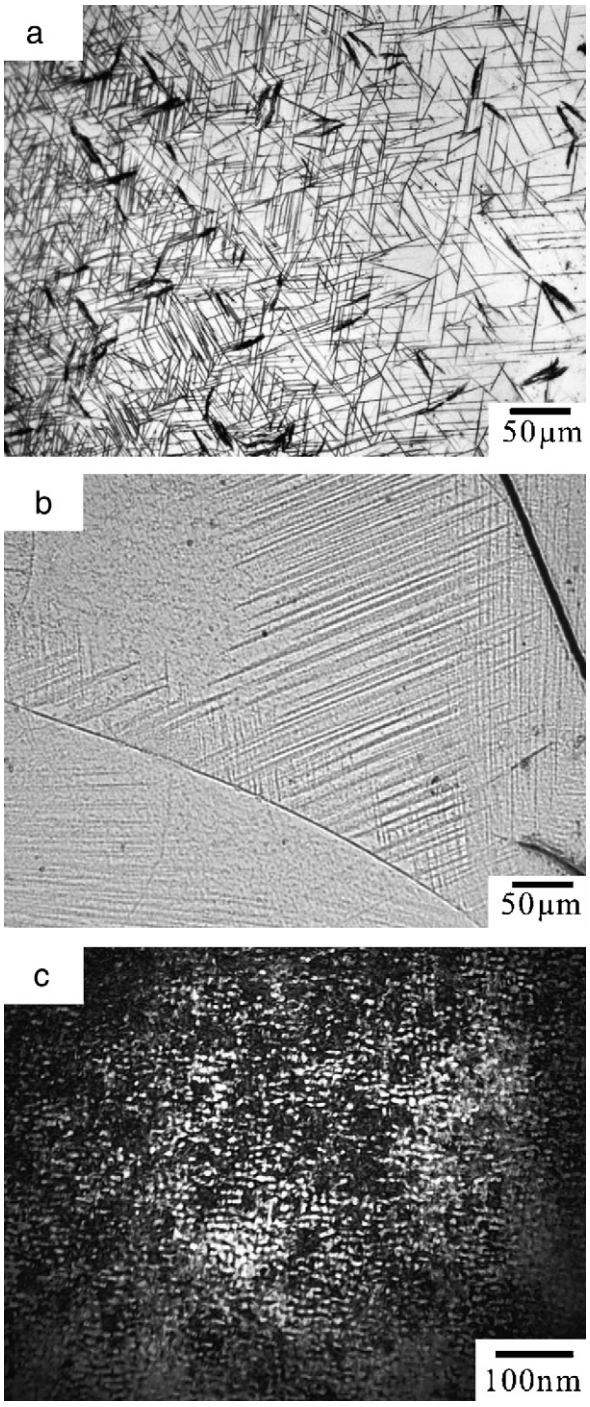

Fig. 2. Microstructures of (a) sample B (≈5 mm in thickness) and (b) sample C (≈1 mm in thickness) quenched from 1380 °C. (c) BFI taken from the $[1\,1\,0]_{bcc}$ direction of the parent phase for sample C quenched from 1380 °C.

Fig. 4 shows the BFI of the sample C quenched from 1380 °C observed in the same area of Fig. 2(b). Although a martensite-like microstructure was observed by optical microscopy, no martensite phase could be detected by TEM observation and only dislocation arrays which were probably introduced along interfaces among some martensite variants, were observed as indicated by yellow

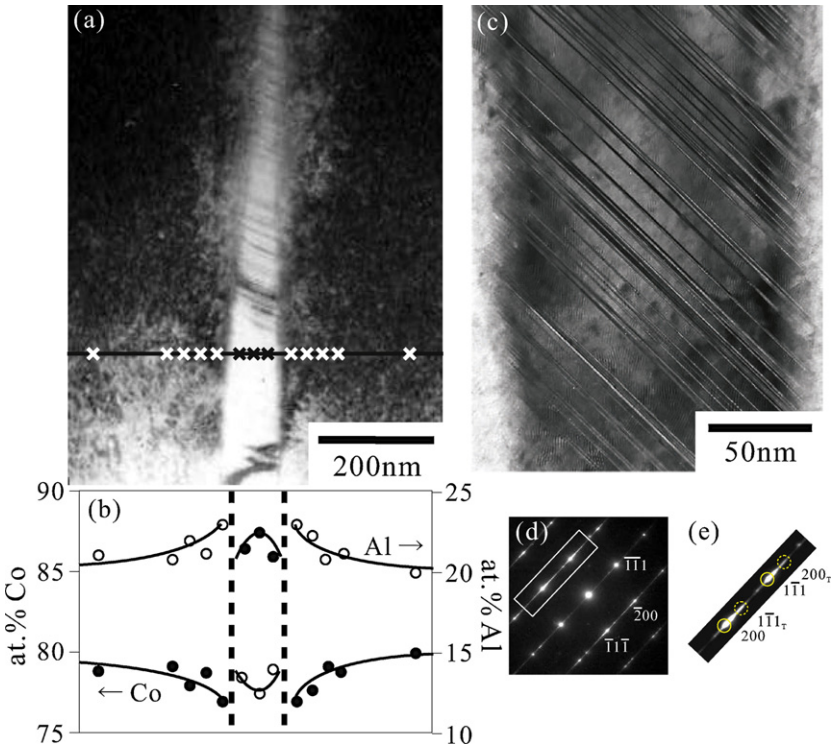

Fig. 3. (a) BFI taken from the $[1\,1\,0]_{bcc}$ direction of sample A quenched from 1380 °C. (b) Composition analysis along the line in (a) by TEM-EDS. (c) A higher magnification BFI for a plate and (d) corresponding SADP taken from $[0\,1\,1]_{fcc}$ direction. (e) The image of the same area as the square in (d) with higher magnification and contrast. Solid and dashed circles have a twin relation.

broken lines in Fig. 4. These results strongly suggest that the martensite phase appears during cooling at least. However, the reason why the martensite phase disappears before the end of quenching is not clear. Further investigations are required to clarify the origin of this microstructure.

3.2. Phase transformations induced by heat treatment

Fig. 5(a) shows the DSC heating curves for sample C quenched from 1380 °C at heating rates of 1, 5 and 10 °C/min. In the case of the heating rate of 10 °C/min, whereas no endothermic peak corresponding to reverse martensitic transformation was detected in the measured temperature region, two exothermal peaks at about 515 °C and 600 °C and one endothermic peak at about 850 °C were

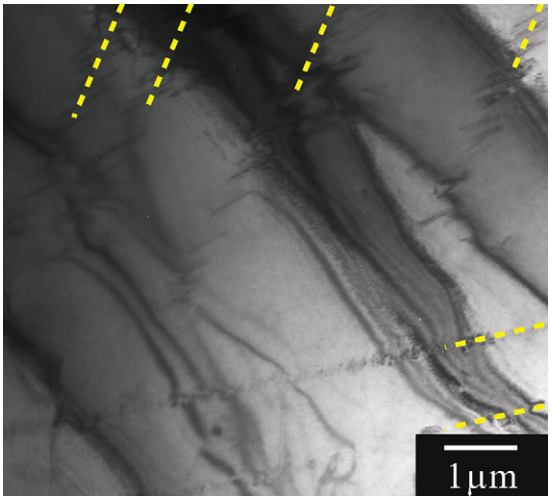

Fig. 4. BFI from the $[1\,1\,0]_{bcc}$ direction of sample C quenched from 1380 °C.

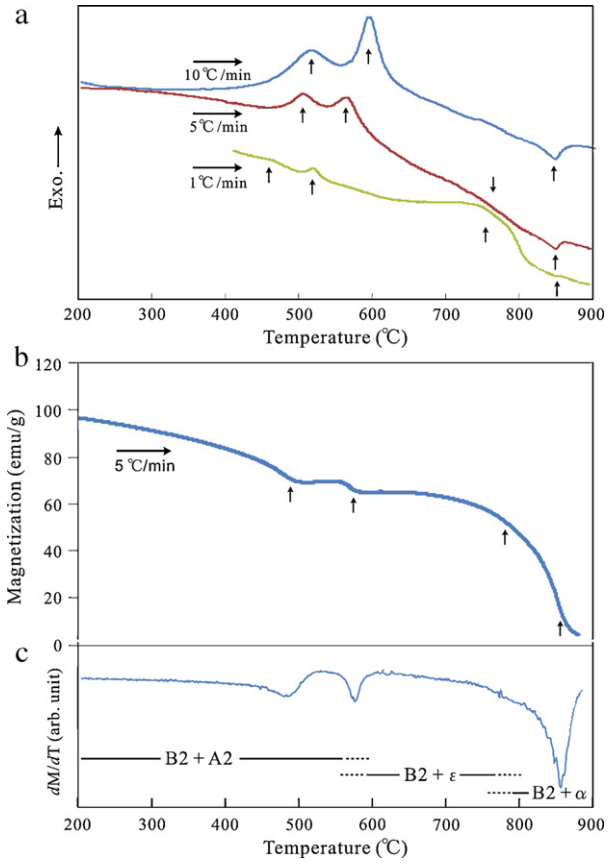

Fig. 5. (a) DSC curves obtained at heating rates of 1, 5 and 10 °C/min for as-quenched sample C. (b) Thermomagnetization (*M*–*T*) curve and (c) its derivation curve obtained at a heating rate of 5 °C/min under a magnetic field of 1 T for the as-quenched sample C.

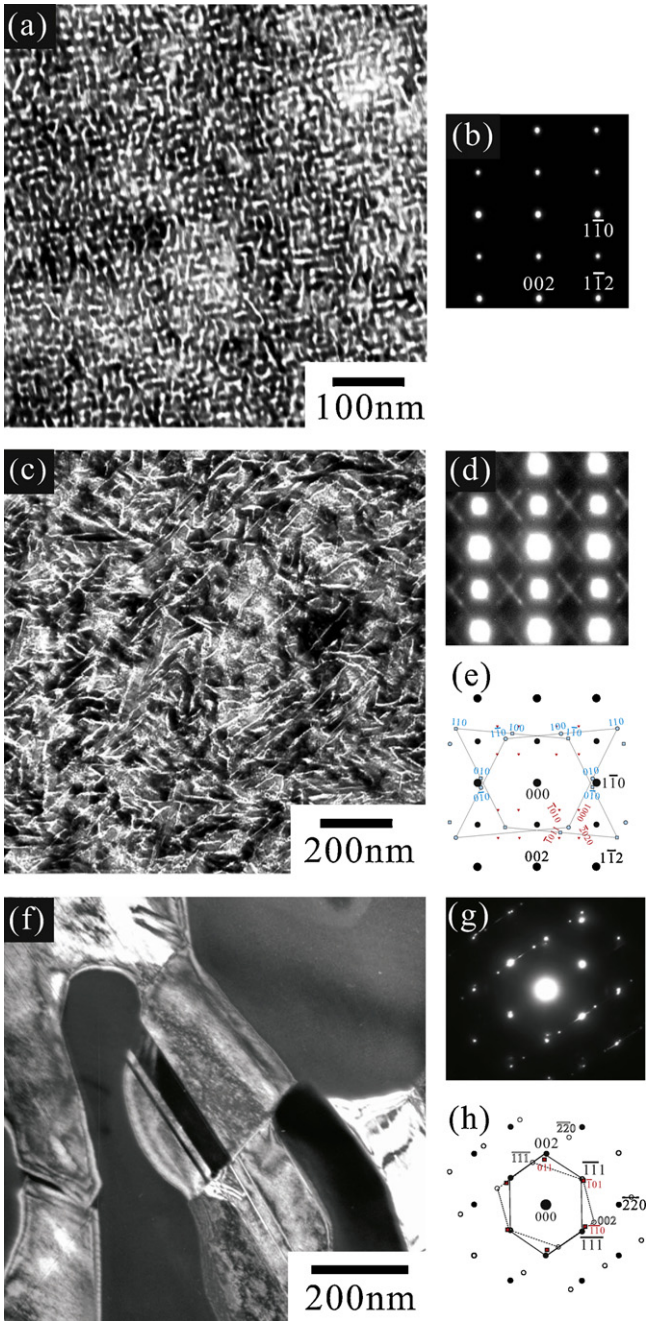

Fig. 6. (a) BFI and (b) corresponding SADP taken from sample C heated from RT to 530 °C at a heating rate of 10 °C/min, the incident beam being $[1\,1\,0]_{bcc}$. (c) BFI and (d) corresponding SADP taken from the sample C heated from RT to 620 °C at a heating rate of 10 °C/min, the incident beam being $[1\,1\,0]_{bcc}$. (e) Key diagram showing ε phase of two variants (open circles and squares), ω phase (triangles) and B2 matrix (closed circles). (f) DFI from $[0\,0\,2]_{\alpha}$ reflection and (g) corresponding SADP taken from the sample C heated from RT to 900 °C at a heating rate of 10 °C/min, the incident beam being $[1\,1\,1]_{fcc}$. (h) Key diagram showing α phase of two variants (open and closed circles) and B2 matrix (open squares).

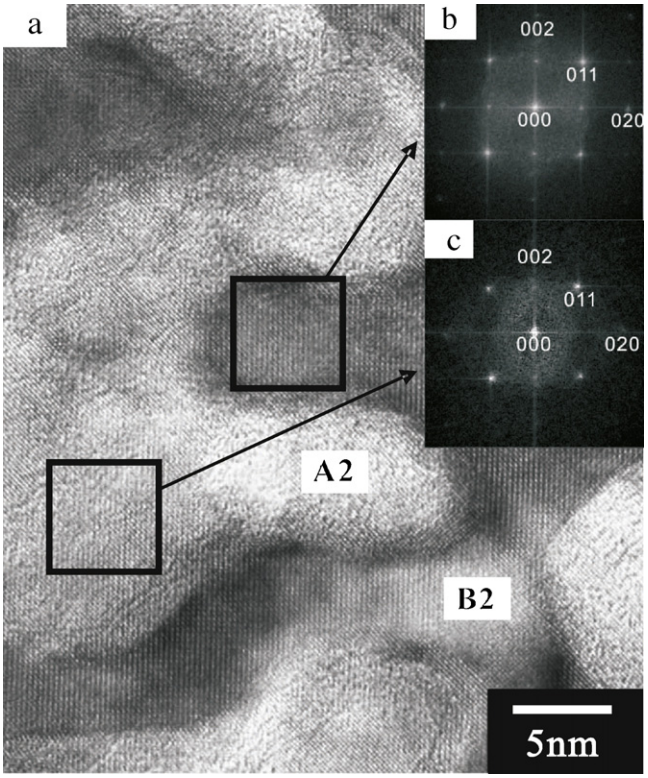

Fig. 7. (a) HREM micrograph taken from $[1\,0\,0]_{bcc}$ direction of the sample C heated from RT to 530 °C. (b and c) FFT images taken from the surrounded areas in (a).

obtained. The intensities and temperatures of the two exothermic peaks decrease with decreasing heating rates, while the endothermic peak is hardly affected by the rate. An additional broad exothermic peak is clearly observed in the temperature region from 650 °C to 800 °C at a heating rate of 1 °C/min, although being faint in the curves at the higher rates. Fig. 5(b) and (c) shows the thermomagnetic (*M*–*T*) curve in the magnetic field of 1 T and its derivation curve of sample C quenched from 1380 °C. The changes in magnetization and its derivation curves are consistent with the results of the DSC examination. The details will be discussed in Section 3.3.

Fig. 6(a) and (b) shows the BFI and its corresponding SADP taken from sample C heated from RT to 530 °C at a heating rate of 10 °C/min followed by water-quenching, where this heat treatment is the same as the thermal history of DSC measurement. While Fig. 6(b) indicates a typical ⟨1 1 0⟩ pattern taken from the B2 structure, the microstructure obviously shows a very fine two-phase structure as shown in Fig. 6(a). This microstructure is similar to that of the as-quenched specimen shown in Fig. 2(c). The second phase with a bright contrast is clearly coarsened. In order to determine the kind of precipitate phase, the dark-field technique using $\{1\,0\,0\}_{B2}$ superreflections in Fig. 6(b) was carried out. However, it was difficult because of the etching effect in jet-polishing. Therefore, HREM observation was carried out using the same specimen as that in Fig. 6(a). Fig. 7(a) shows the HREM image, and Fig. 7(b) and (c) exhibits the fast Fourier transformation (FFT) patterns taken from the two different regions with dark and bright contrasts, respectively, surrounded by the square symbols in Fig. 7(a). The FFT pattern taken from the dark area (Fig. 7(b)) shows $\{1\,0\,0\}_{B2}$ superreflections, while those superreflections are missing in Fig. 7(c) taken from the bright area. This means that the phases with the dark and bright contrasts have B2 and A2 structures, respectively, and that the exothermal peak at about 515 °C is induced by the progress of the phase separation into the A2 + B2 structure. It is reasonable that the phase separation occurs in Co–21 and –23 at.% Al alloys during quenching from 1380 °C as shown in Fig. 2(c), because the A2 phase with the disordered crystal structure of the B2 parent phase seems to be easily introduced by spinodal decomposition while going through the metastable A2 + B2 two-phase region shown in Fig. 1.

Fig. 6(c) and (d) shows the BFI and its corresponding SADP taken from sample C heated from RT to 620 °C as well as the thermal history of DSC measurement, respectively, where the key diagram

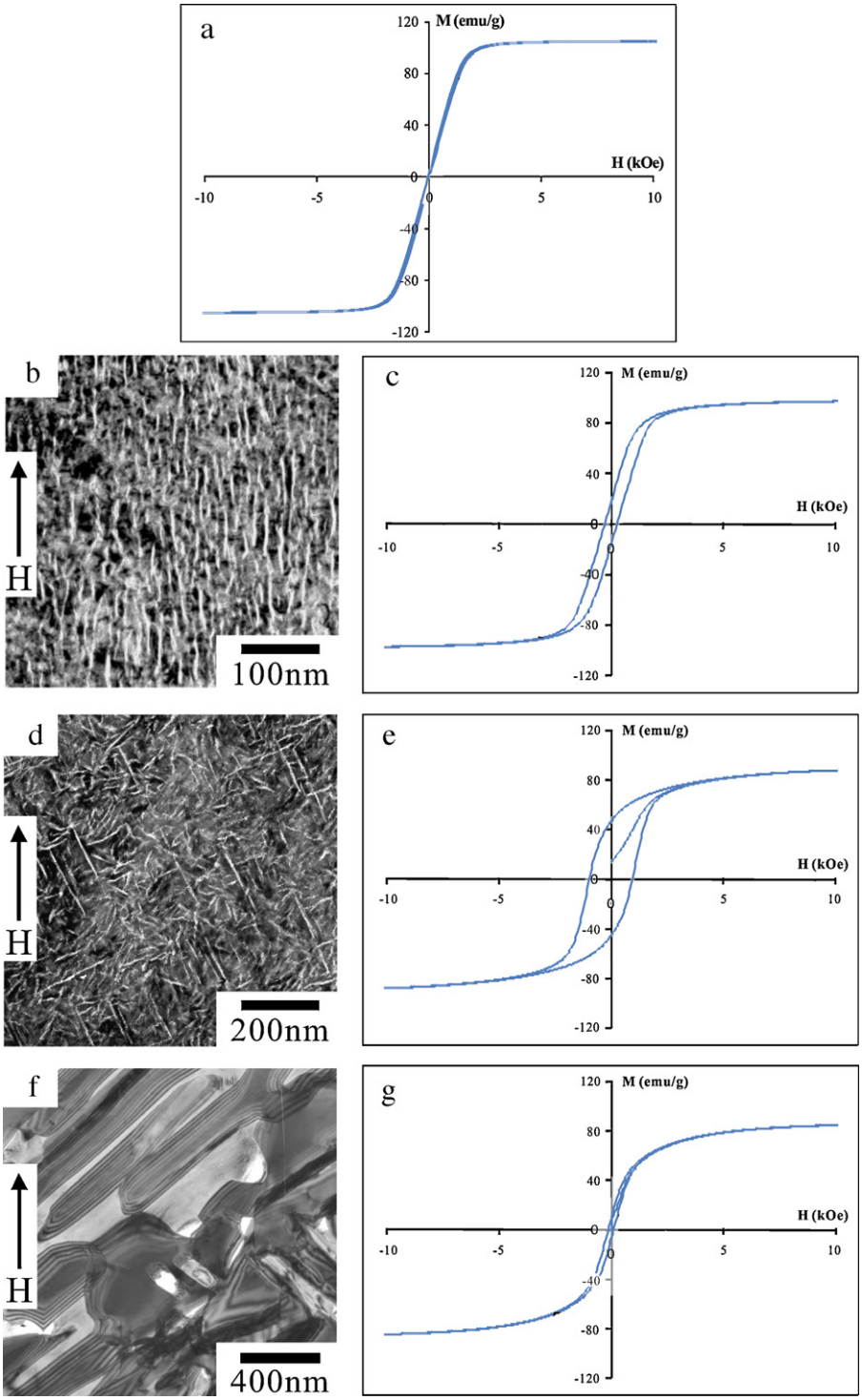

Fig. 8. Magnetization curves of sample C (a) as-quenched from 1380 °C and subsequently heated from RT to (c) 530 °C, (e) 620 °C and (g) 900 °C at a heating rate of 5 °C/min under a magnetic field of 1 T followed by air-cooling. (b, d and f) BFIs taken from $[1\,1\,0]_{bcc}$ zone axis of the specimens whose magnetic properties are presented in (c), (e) and (g), respectively.

for Fig. 6(d) is also indicated in Fig. 6(e). The microstructure of the second phase in the 620 °C specimen becomes thinner than that in the 530 °C specimen and many extra spots indexed with hcp and ω structures, besides the spots from the B2 phase, were detected. Due to the similarity of the morphology [6,7], the precipitate phase with the bright contrast may be the ε phase. Consequently, the exothermic reactions at about 515 °C and 600 °C are caused by the progress of the A2 + B2 phase separation and by the precipitation of the ε and ω phases, respectively.

Fig. 6 (f)–(h) shows the BFI, the corresponding SADP and its key diagram taken from sample C heated from RT to 900 °C, respectively. The microstructure is further coarsened and from Fig. 6(h), it was confirmed that this specimen is composed of the α and β in the Kurdjumov–Sachs OR. Here, we can recognize a twin-like microstructure in the α phase and this structure was found to correspond to the spots with open circles in Fig. 6(h). Because {1 1 1} planes of the β phase have four equivalent variants, the α phase may be subject to precipitate along the variants of {1 1 1} planes of

the β phase at the initial stage of α phase precipitation. Martensitic transformation from the α phase to the ε phase has been reported [2], but no diffraction patterns corresponding to the hcp phase is observed in the α phase in this study. This result suggests that martensitic transformation is inhibited by the size effect as the α phase has a fine structure (∼200 nm). The exothermic peak appearing at temperatures ranging from 650 °C to 800 °C in the DSC curve of Fig. 5(a) is concluded to be due to the precipitation of the stable α phase.

3.3. Magnetic properties of Co–23 at.% Al alloy

It is known that the Co–Al alloys exhibit coercivity [1] due to the precipitation of the ferromagnetic metastable ε phase in the paramagnetic β phase [7,8]. However, the β phase has also been reported to become ferromagnetic in low Al contents under 27 at.% Al [15] and the metastable A2 phase is also expected to be ferromagnetic [11]. Actually, as shown by the thermomagnetizatioin curve of Fig. 5(b), the as-quenched sample with the metastable A2 + B2 two-phase structure shows ferromagnetism. The thermomagnetization curve of sample C shown in Fig. 5(b) and (c) indicates two small decremental points in magnetization at 482 °C and 573 °C, and a disappearance of magnetization at 856 °C, where the characteristic temperatures are defined by the local minimum value of dM/dT shown in Fig. 5(c). The former two changes at 482 °C and 573 °C are roughly coincident with the exothermal peaks due to the precipitation of the A2 and ε phases, respectively, shown in Fig. 5(a). The magnetization in the A2 + β two-phase region at RT decreases with increasing temperature and it is therefore considered that the plateaus followed by the two points at 482 °C and 573 °C are caused by the progress of the precipitation of the ferromagnetic A2 phase and by the formation of the ferromagnetic ε phase, respectively. It is also seen that the dM/dT decreases at about 770 °C, which is probably due to the formation of the stable α phase. The decrease in the magnetization at 856 °C is the Curie temperature (T_c) of α phase, which is in good agreement with a reported value shown in Fig. 1. These results mean that the A2 and ε phases precipitating in the paramagnetic B2 matrix are ferromagnetic at room temperature and that some coercivity can be expected in these two-phase alloys as well as in Malcolloy [1].

Fig. 8(a), (c), (e) and (g) shows the magnetization (MH) curves obtained from sample C (a) as-quenched, and subsequently heated to (c) 530 °C, (e) 620 °C and (g) 900 °C at a heating rate of 5 °C/min under a magnetic field of 1 T, where the magnetization was measured in the direction parallel to that of the magnetic field during aging. The BFIs in the specimens giving the MH curves of Fig. 8(c), (e) and (g) are also shown in Fig. 8(b)–(f), respectively. While hardly detected in the as-quenched sample of Fig. 8(a) and in the overheated sample of Fig. 8(g), some coercivity was detected in the specimens heated to 530 °C and 620 °C as shown in Fig. 8(c) and (e). In these specimens, the fine A2 and ε particles tend to elongate in the direction of the applied field, as shown in Fig. 8(b) and (d), respectively, and this kind of microstructure is much more remarkable in Fig. 8(b). On the other hand, in the specimen heated to 900 °C, the α + β two-phase microstructure is significantly coarsened, as shown in Fig. 8(f). The coercivity of about 960 Oe in the β + ε structure is comparable to that in the Marcolloy and larger than that of about 300 Oe in the β + A2 structure, as shown in Fig. 8(c) and (e). This difference is due to the difference in the origin of coercivity between them. In the case of the β + A2 structure, the coercivity is brought about by the shape anisotropy of the prolonged A2 phase particles. However, that of the β + ε structure is apparently due to the high crystalline anisotropy energy of the ε particles with the low symmetric hcp structure.

4. Conclusions

Phase transformations from the β phase were investigated in Co–21 and –23 at.% Al alloys and the following results were obtained.

1. The Co–Al alloys with low Al content exhibit martensitic and bainitic transformations, depending on the quenching condition. The bainite phase with the fcc structure could be observed in the thick specimen with lower quenching rate. The composition of the bainite plate was experimentally determined to be about Co–13 at.% Al. On the other hand, a martensite-like structure could be partially recognized in the thin specimens with higher quenching rate.
2. The parent phase of the as-quenched specimens showed the phase separation into the metastable A2 + B2 structure, which progresses by additional heating. Subsequently, this A2 phase transforms to the metastable ε phase and then finally changes to the stable α phase.
3. The as-quenched thin specimen with the A2 and B2 structure exhibits ferromagnetism, while it shows some coercive force after additional heating up to 530 °C under a magnetic field of 1 T. This coercive force is thought to be induced by the A2 precipitates elongated by the applied field.

Acknowledgements

This study was supported by a Grant-in-Aid for Scientific Research from the Japan Society for the Promotion of Science (JSPS) and New Energy and Industrial Technology Development Organization (NEDO), Japan. The support from the Global COE Project is also acknowledged.

References

[1] H. Masumoto, T. Kobayashi, K. Watanabe, Trans. JIM 6 (1965) 187–191.
[2] T. Omori, Y. Sutou, K. Oikawa, R. Kainuma, K. Ishida, Mater. Trans. 44 (2003) 2732–2735.
[3] T. Omori, Y. Sutou, K. Oikawa, R. Kainuma, K. Ishida, Scripta Mater. 52 (2005) 565–569.
[4] J. Sato, T. Omori, K. Oikawa, I. Ohnuma, R. Kainuma, K. Ishida, Science 312 (2006) 90–91.
[5] A.J. McAlister, in: T.B. Massalski (Ed.), Binary Alloy Phase Diagrams, second ed., ASM International, 1990, p. 136.
[6] T. Omori, Y. Sutou, K. Oikawa, R. Kainuma, K. Ishida, Mater. Sci. Eng. A 438 (2006) 1045–1049.
[7] R.E. Johnson, H.W. Rayson, W. Wright, Acta Metall. 20 (1972) 387–397.
[8] A.M. Zeltser, W.A. Soffa, IEEE Trans. Mag. MAG-22 (1986) 588–590.
[9] H. Ohtani, Y. Chen, M. Hasebe, Mater. Trans. 45 (2004) 1489–1498.
[10] T. Kozakai, T. Shikama, T. Koyama, M. Doi, Mater. Sci. Forum 61 (2004) 449–452.
[11] N. Kamiya, T. Sakai, R. Kainuma, I. Ohnuma, K. Ishida, Intermetallics 12 (2004) 417–423.
[12] R. Kainuma, M. Ise, C.C. Jia, H. Ohtani, K. Ishida, Intermetallics 4 (1996) S151–158.
[13] K. Oikawa, L. Wulff, T. Iijima, F. Gejima, T. Ohmori, A. Fujita, K. Fukamichi, R. Kainuma, K. Ishida, Appl. Phys. Lett. 79 (2001) 3290–3292.
[14] J.L. Smialek, R.F. Hehemann, Metall. Trans. 4 (1973) 1571–1575.
[15] J. Schramm, Z. Metallkd. 33 (1941) 381–387.